High performance of solution-processed SnO 2 thin-film transistors by promotion of photo-exposure time-dependent carrier transport during the pre-annealing stage

Jun-Ik Park, Do-Kyung Kim, Hyunjae Lee, Jaewon Jang, Jihwan Park, Hyeok Kim, Philippe Lang, In Man Kang, Jin-Hyuk Bae

Semiconductor Science and Technology

PAPER

High performance of solution-processed SnO_2 thin-film transistors by promotion of photo-exposure time-dependent carrier transport during the pre-annealing stage

To cite this article: Jun-Ik Park *et al* 2020 *Semicond. Sci. Technol.* **35** 065019

IOP Publishing Semiconductor Science and Technology
Semicond. Sci. Technol. **35** (2020) 065019 (7pp) https://doi.org/10.1088/1361-6641/ab8537

High performance of solution-processed SnO_2 thin-film transistors by promotion of photo-exposure time-dependent carrier transport during the pre-annealing stage

Jun-Ik Park[1], Do-Kyung Kim[1], Hyunjae Lee[1], Jaewon Jang[1], Jihwan Park[1], Hyeok Kim[2], Philippe Lang[3], In Man Kang[1] and Jin-Hyuk Bae[1,4]

[1] School of Electronics Engineering, Kyungpook National University, 80 Daehakro, Bukgu, Daegu 41566, Republic of Korea
[2] Department of Electrical and Computer Engineering, University of Seoul, 163 Seoulsiripdaero, Dongdaemun-gu, Seoul 02504, Republic of Korea
[3] ITODYS, CNRS UMR 7086, Université Paris Diderot (Paris7), 15 rue Jean-Antoine de Baïf, 75205, Paris CEDEX 13, France

E-mail: jhbae@ee.knu.ac.kr

Received 28 December 2019, revised 14 February 2020
Accepted for publication 31 March 2020
Published 21 May 2020

Abstract

We fabricate high-performance solution-processed SnO_2 thin-film transistors (TFTs) exhibiting improved carrier transport features by exposing the ultraviolet/ozone (UV/O_3) on the SnO_2 film during the pre-annealing stage. The SnO_2 layer is treated with different UV/O_3-exposure times from 0 to 60 minutes before the post-annealing step. As UV/O_3-exposure time increases from 0 to 30 minutes, the M-O-M (M, metal; and O, oxygen) network, mass density, and oxygen vacancies of films are enhanced. In contrast, the M-O-M network and mass density decrease, while the oxygen vacancies rather increase when the UV/O_3-exposure time reaches 60 minutes beyond 30 minutes. The SnO_2 (Sn^{4+}) phase, thickness, and surface morphology of SnO_2 films are not considerably changed regardless of UV/O_3-exposure time. When the UV/O_3-exposure time is 30 minutes, devices demonstrate superior field-effect mobility (10.1 $cm^2\ V^{-1}\ s^{-1}$) at approximately two times higher than the TFT without UV/O_3-exposure. Furthermore, the SnO_2 TFT with UV/O_3-exposure time for 30 minutes shows improved subthreshold-swing characteristics and a high on/off current ratio. These devices are adequate for use in high-resolution active-matrix LCDs or OLED displays that demand a high field-effect mobility (>10 $cm^2\ V^{-1}\ s^{-1}$) and on/off ratio (>10^6).

Keywords: SnO_2, photo-exposure time, solution-process, thin-film transistor, high-performance

(Some figures may appear in colour only in the online journal)

[4] Author to whom any correspondence should be addressed.

1. Introduction

Metal oxide semiconductor-based thin-film transistors (TFTs) have become important as fundamental devices for next-generation displays because they exhibit not only outstanding electron mobility but also high transparency in the visible light regime compared with conventional silicon (Si)-based TFTs [1–4]. Among the different metal oxides, binary oxide semiconductors including indium(III) oxide (In_2O_3), zinc oxide (ZnO), and tin(IV) oxide (SnO_2) show higher electrical conductivity than the other insulating ionic compounds [5–7]. Many investigators have recently turned to Sn-based oxide TFT because indium (In) is toxic, a rare earth element, and costly [8, 9]. Furthermore, the SnO_2 semiconductor has many advantages such as a wide optical band gap, crystallization at relatively low temperatures, and remarkable charge transport properties via heavy-metal cations with $(n-1)d^{10}ns^0$ ($n \geqslant 5$) electronic configurations, leading to the impressive electrical performance of SnO_2 TFTs [10–12]. On the other hand, oxide semiconducting materials can be formed into thin-film by both a vacuum process and a solution process [13–16]. From the viewpoint of vacuum-free deposition, the solution process is cost-effective, simple, and applicable to spin-coating, inkjet printing, and meniscus-guided coating, suitable for large-scale production [17–20]. The solution-process inevitably requires a pre-annealing step to evaporate residual solvent on coated films before post-annealing with a relatively high-temperature to develop the active layer [21, 22]. The pre-annealing temperature leads to an endothermal reaction related to the precursor dissociation and subsequent hydrolysis reaction that generates M-OH bonding (M, metal; O, oxygen; and H, hydrogen) which could be converted to M-O-M network bonding through dehydration and alloying reactions during the post-annealing step [21–23]. In this regard, researching pre-annealing treatment is important for improving the electrical performance of oxide TFTs. However, many studies have focused on post-annealing treatments such as high-pressure annealing, ambient gas control, and water vapor annealing [24–26].

In this study, we fabricated high-performance TFTs by controlling ultraviolet/ozone (UV/O_3)-exposure time on solution-processed SnO_2 films during the pre-annealing stage. The change of molecular structure, crystallinity, and morphological characteristics of solution-processed SnO_2 thin-films with different UV/O_3-exposure times from 0 to 60 minutes was systematically investigated. We observed the enhanced physical- and chemical characteristics of SnO_2 films that show increased mass density, M-O-M network, and oxygen vacancies when the UV/O_3-exposure time is 30 minutes. In contrast, mass density and M-O-M network decreased, while the oxygen vacancies rather excessively increased when UV/O_3-exposure time reached 60 minutes beyond 30 minutes. The crystalline size, thickness, and surface roughness of SnO_2 films were similar regardless of UV/O_3 treatment. The SnO_2 TFT with UV/O_3 treated for 30 minutes demonstrated superior electrical properties with the highest field-effect mobility of 10.1 $cm^2\ V^{-1}\ s^{-1}$ and on/off current ratio of 1.2×10^6, adequate for use in high-resolution active-matrix LCDs or OLED displays [27].

2. Methods

2.1. Fabrication process

A schematic for the fabrication process of a coplanar bottom-gate SnO_2 TFT with UV/O_3 treatment is depicted in figure 1. A heavily boron-doped p-type Si wafer and thermally grown 100 nm SiO_2 were used as the gate electrode and gate insulator, respectively. For the bottom contact structure, 50 nm thick Au electrodes were deposited on SiO_2 using e-beam evaporation and then patterned by the lift-off method to design an active channel layer with a length of 1 000 μm and width of 100 μm. The Si/SiO_2 substrate was cleaned by UV/O_3 for 60 minutes before spin-coating. The solution for the SnO_2 active materials was prepared by dissolving 0.025 M of tin(II) chloride dihydrate ($SnCl_2 \cdot 2H_2O$) in ethanol. The prepared solution was spin-coated at 3000 rpm for 50 s onto a Si/SiO_2 substrate followed by pre-annealing at 150 °C for 10 minutes to evaporate the residual solvent. In a previous study, SnO_2 films coated with ethanol-based chloride precursor solution dried at 150 °C demonstrated suitable environmental stability with high densification [28].

UV irradiation (25 mW cm^{-2}) was conducted with a low-pressure mercury lamp with two types of light sources (Jaesung engineering, UVC-30). One had a wavelength of 184.9 nm and an energy of 647 kJ mol^{-1}, and the other had a wavelength of 253.7 nm and an energy of 472 kJ mol^{-1}. These two light source energies are larger than the bonding energy of the contaminant organic and hydrogen compounds such as C-C (348 kJ mol^{-1}), C-O (352 kJ mol^{-1}), C-H (413 kJ mol^{-1}), and O-H (463 kJ mol^{-1}). Moreover, these light sources continuously produce O_3 and oxygen free radicals ($O(^3p)$ and $O(^1D)$) through the following reactions [29, 30]:

$$O_2 + hv\,(185\ nm) \rightarrow O\left(^3P\right) + O\left(^3P\right) \quad (1)$$

$$O_2 + O\left(^3P\right) \rightarrow O_3 \quad (2)$$

$$O_3 + hv\,(254\ nm) \rightarrow O\left(^1D\right) + O_2. \quad (3)$$

As presented in Equations (1) and (3), Ozone (O_3) and excited singlet atomic oxygen ($O(^1D)$) are strong oxidants and easily eliminate organic contaminants as volatile byproduct molecules such as CO_2, H_2O, and O_2 [29]. The UV/O_3-exposure time was adjusted at 0, 15, 30, 45, and 60 minutes to explore the effect of UV/O_3-exposure on SnO_2 film and obtain the high electrical performance of a SnO_2 TFT. After the pre-annealing stage with UV/O_3-exposure, post-annealing was performed at 450 °C for 1 h in a tube furnace with ambient air to remove organic residues, activate metal oxide film, and assist crystallization of SnO_2. The coated films were mechanically eliminated in advance before measurement of the electrical performance in the SnO_2 TFT for complete

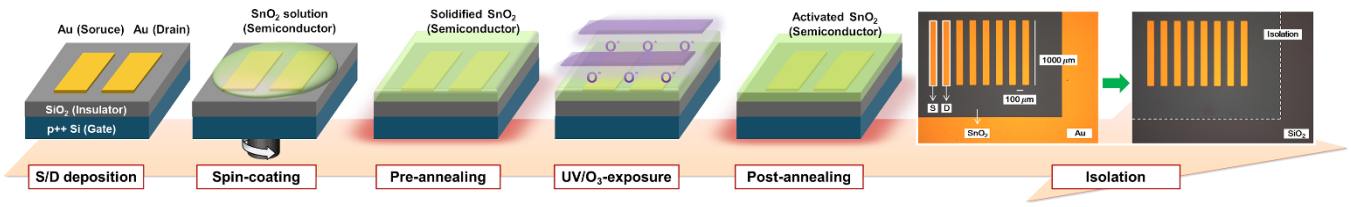

Figure 1. A schematic for the fabrication process of the coplanar-bottom gate UV/O_3-exposed SnO_2 TFT.

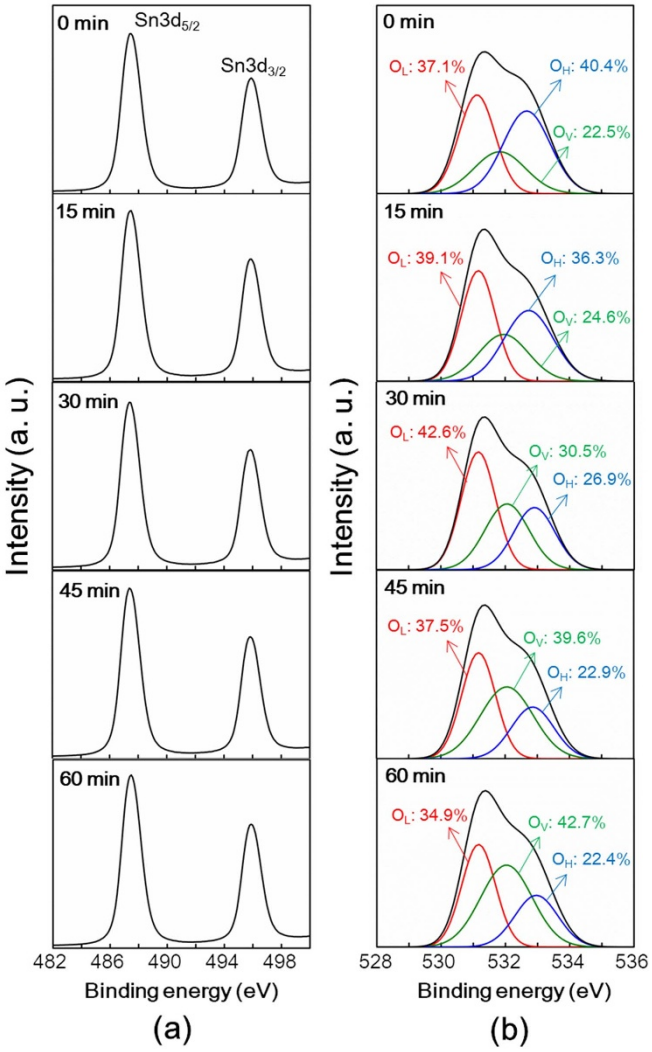

Figure 2. XPS spectra of (a) Sn 3d and (b) O 1 s state of SnO_2 films with different UV/O_3-exposure times.

isolation to minimize gate leakage current and fringing effect. The optical images before and after the isolation of the device are shown in figure 1.

2.2. Analysis method

x-ray photoelectron spectroscopy (XPS) (ThermoFisher Scientific, NEXSA) was conducted using a monochromatic Cu Kα (1.5418 Å) light source to observe the surface electronic states and chemical compositions of SnO_2 films. The mass density and thickness of the films were investigated with x-ray reflectivity (XRR) (Panalytical, Empyrean) analysis and

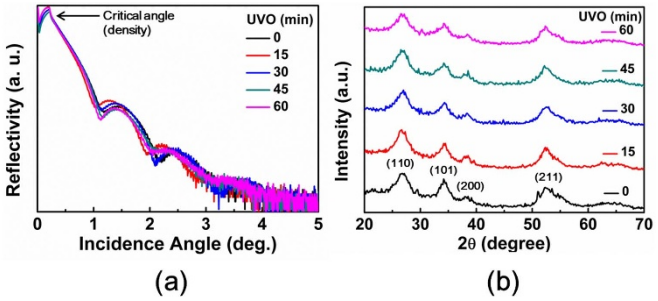

Figure 3. (a) XRR spectra and (b) GIXD patterns of SnO_2 films with different UV/O_3-exposure times.

simulation using commercial software (X'Pert Reflectivity). The crystallization behavior of SnO_2 films was examined using grazing incidence x-ray diffraction (GIXD) (Panalytical, Empyrean). The surface morphology of the films was obtained through atomic force microscopy (AFM) (NX20, Pary Systems) in non-contact mode. The electrical properties of the SnO_2 TFTs were measured using a source measure unit (Keithley 2636B, Tektronix) and a probe station (MSTECH, MST 4000A) under atmospheric pressure in a dark space.

3. Results and discussions

Figures 2(a) and (b) present the XPS spectra of Sn 3d and O 1 s peaks of SnO_2 films with different UV/O_3-exposure times. Based on the Sn 3d core level in figure 2(a), the peak positions of $Sn3d_{5/2}$ and $Sn3d_{3/2}$ for all films occurred at 487.4 and 495.8 eV, consistent with the typical SnO_2 (Sn^{4+}) phase [31, 32]. There was no shift in the binding energy of Sn peaks irrespective of UV/O_3-exposure time, indicating that UV/O_3-exposure on SnO_2 films during the pre-annealing stage did not affect the phase transition between SnO_2 and SnO. The O 1 s state is divided into three peaks associated with lattice oxygen (O_L, denoting the M-O-M network for the electron path), oxygen-vacancies (O_V, denoting free carrier concentration), and hydroxyl groups (O_H, denoting the electron trap site) at 531.1, 532.0, and 532.8 eV, using Gaussian fitting as depicted in figure 2(b) [33]. As the UV/O_3-exposure time increase, the O_H ratio decreased and the O_V ratio increased because UV irradiation and the oxidation by both O_3 and oxygen-free radicals contribute to decompose the residual hydrogen compounds and then removed as volatile products. When the UV/O_3-exposure time was 30 minutes, the O_L ratio was highest because of improved the M-O-M network formations and reorganization through reduced carbon-based

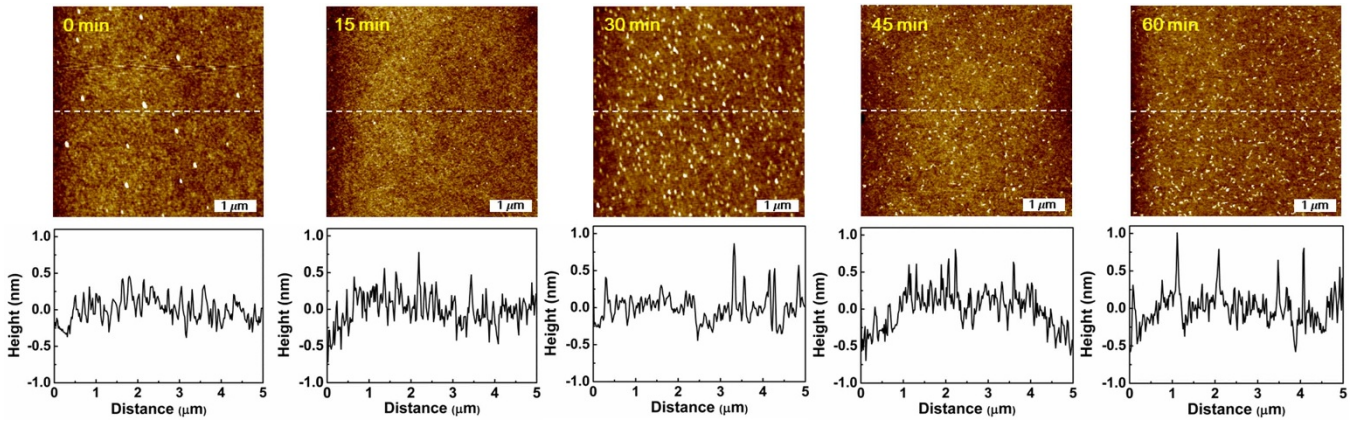

Figure 4. AFM images (5 × 5 μm) and corresponding cross-sectional height profiles of SnO_2 films with different UV/O_3-exposure times.

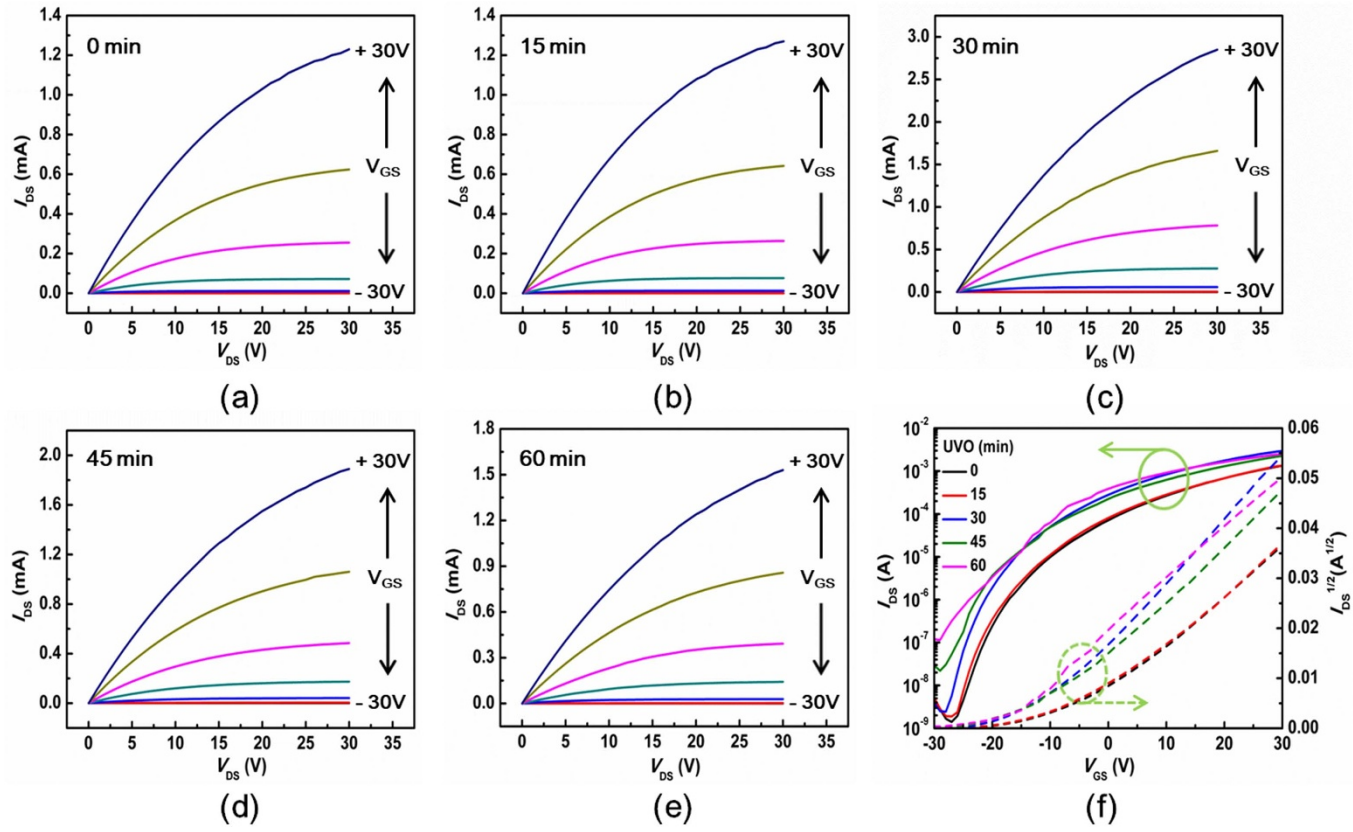

Figure 5. (a)–(e) Output and (f) transfer characteristics of SnO_2 TFTs with different UV/O_3-exposure times.

content [16]. However, the O_L ratio was reduced by eliminating too many hydrogen compounds which could be involved in formation of the M-O-M network via condensation reactions when the UV/O_3-exposure time exceeded 30 minutes. Figure 3(a) illustrates the XRR curves of SnO_2 films with different UV/O_3-exposure times and arrow means the point where the critical angle was determined using X'Pert Reflectivity software. Accordingly, we extracted the critical angle to calculate the mass density of SnO_2 thin-films using following equation:

Table 1. The critical angle, mass density and RMS roughness of the SnO_2 films with different UV/O_3-exposure times.

UV/O_3-exposure time (min)	Critical angle (deg)	Mass density (g cm^{-3})	RMS roughness (nm)
0	0.2417	3.17	0.20
15	0.2420	3.18	0.21
30	0.2613	3.71	0.24
45	0.2680	3.90	0.26
60	0.2424	3.19	0.32

Table 2. The electrical properties of the SnO_2 TFTs and their standard deviations with different UV/O_3-exposure times.

UV/O_3-exposure time (min)	Field-effect mobility ($cm^2\ V^{-1}\ s^{-1}$)		On/off ratio		Subthreshold swing (V/decade)	
	Mean	Std. Dev.	Mean	Std. Dev.	Mean	Std. Dev.
0	5.95	0.43	8.3×10^5	1.2×10^5	2.53	0.20
15	6.31	0.59	9.4×10^5	2.3×10^5	2.13	0.21
30	9.81	0.57	1.1×10^6	2.2×10^5	1.98	0.24
45	6.92	0.64	1.4×10^5	3.5×10^4	3.55	0.29
60	5.46	0.84	4.7×10^4	1.3×10^4	3.73	0.45

Table 3. Performance comparison of the various solution-processed SnO_2 TFTs.

Ref.	Gate insulator	Capacitance per unit area ($nF\ cm^{-2}$)	Annealing conditions	Channel length/width (μm)	μ_{sat} ($cm^2\ V^{-1}\ s^{-1}$)	On/off I_{DS} ratio
This work	SiO_2	34.5	450 °C for 1 h	100/1000	10.1	10^6
[38]	SiO_2	11.5	450 for 4 h	100/600	0.37	10^6
[39]	SiO_2	11.5	450 for 4 h	100/600	0.19	10^3
[12]	SiO_2	31.4	500 for 1 h	5/110	0.23	10^6
[40]	SiO_2	34.5	600 for 4 h	100/1000	10.87	10^7
[41]	Al_2O_3	225	450 for 30 min	60/1400	96.4	10^6

$$\theta_c = \lambda\sqrt{\rho_e r_e/\pi} \tag{4}$$

$$\rho_m = \frac{\rho_e A}{N_A Z} \tag{5}$$

where θ_c is the critical angle, λ is the wavelength of x-ray source (1.5418 Å for Cu Kα), ρ_e is the electron density, r_e is the classical radius of the electron (2.818×10^{-13} cm), ρ_m is the mass density, A is the atomic weight (150.71 g mol^{-1} for SnO_2), N_A is Avogadro's number (6.023×10^{23} mol^{-1}), and Z is the atomic number (66 for SnO_2) [34, 35]. While increasing the UV/O_3-exposure time from 0 to 45 minutes, the mass density of SnO_2 films increased from 3.17 to 3.90 g cm^{-3} owing to eliminating organic residue. However, the mass density of SnO_2 films decreased to 3.19 g cm^{-3} when the UV/O_3-exposure time was 60 minutes because the reduced M-O-M network by hydrogen compounds are excessively decomposed, as mentioned in the XPS analysis. Regardless of UV/O_3-exposure time, the thickness of all SnO_2 films was approximately 4.53 nm ±3.6 Å, calculated with the periodicity of the fringes using XRR simulation. These values are similar to the thickness analyzed by transmission electron microscopy (TEM) in a previous study [11]. We conducted GIXD analysis to investigate the crystallinity of SnO_2 films with different UV/O_3-exposure times, as depicted in figure 3(b). All diffraction peaks well-matched a tetragonal rutile SnO_2 pattern (JCPDS 41–1445) and had almost the same shape irrespective of UV/O_3-exposure time. The crystallite size of the films was obtained using the Scherrer formula; all films had a similar crystal size of approximately 7 ± 0.8 Å. Figure 4 illustrates the AFM images and corresponding height profile of SnO_2 films with different UV/O_3-exposure times. The root-mean-square (RMS) roughness increased from 0.20 to 0.32 nm with increasing UV/O_3-exposure time up to 60 minutes. Nevertheless, this small surface damage did not affect the electrical properties of the SnO_2 TFT since values of RMS roughness differed only slightly in the angstrom-range and the TFTs are fabricated with bottom-contact structure. The values of critical angle, mass density, and RMS roughness of SnO_2 films with different UV/O_3-exposure times were summarized in table 1.

Figures 5(a)–(e) exhibit the output characteristics of SnO_2 TFTs with different UV/O_3-exposure times (I_{DS}–V_{DS} curves at V_{GS} from −30 to +30 V with an increment of 10 V). All devices exhibited conventional n-type semiconductor behavior and a normally-turned-on state regardless of UV/O_3-exposure time. Changes in the transfer characteristics (I_{DS}–V_{GS}) of SnO_2 TFT were observed with respect to UV/O_3-exposure time, as depicted in figure 5(f). All the TFTs were operated in the saturation regime by applying a constant V_{DS} of +30 V. As UV/O_3-exposure time increased, the off-current increased and turn-on voltage (V_{ON}) shifted slightly negatively from −26 to −28 V as free carrier concentration increased, associated with O_v. Furthermore, the subthreshold swing characteristics (SS) improved from 2.44 (0 minutes) to 1.83 V/decade (30 minutes) due to reduced organic-based content, whereas SS deteriorated to 4.31 V/decade (60 minutes) since an excessively increased O_v ratio leads to many oxygen deficiency defects and a high off-current [36, 37]. The field-effect mobility was estimated from the following conventional MOS transistor saturation mobility equation:

$$\mu_{sat} = \frac{2L}{WC_i}\left(\frac{\partial\sqrt{I_{sat}}}{\partial V_{Gs}}\right)^2 \tag{6}$$

where C_i is the gate insulator capacitance per unit area and L and W are the channel length and width. While increasing UV/O_3-exposure time from 0 to 30 minutes, the extracted

field-effect mobility increased from 6.27 to 10.1 $cm^2\ V^{-1}\ s^{-1}$ because of the enhanced M-O-M network and mass density of SnO_2 films, leading to the highest on-current (on/off ratio of 1.2×10^6). In contrast, the field-effect mobility decreased to 4.31 $cm^2\ V^{-1}\ s^{-1}$ owing to the reduced M-O-M network and high oxygen deficiency defects. The electrical characteristics of the SnO_2 TFT for different UV/O_3-exposure times are summarized in table 2 with both means and standard deviations deduced from 20 devices for each condition. Table 3 shows the performance comparison of the various solution-processed SnO_2 TFTs with the different fabrication processes. The device of this work exhibits higher field-effect mobility than other studies with a fabrication process analogous to ours (same gate insulator and similar post-annealing temperature). In addition, there is similar field-effect mobility with ours in spite of high post-annealing temperature for a long time. If UV/O_3-exposure is applied to other SnO_2 TFTs with high-k gate insulator or high post-annealing temperature, the electrical performance would be improved as in this work.

4. Conclusion

High-performance solution-processed SnO_2 TFTs were fabricated by the controlling of UV/O_3-exposure on films during the pre-annealing stage. We identified the optimal UV/O_3-exposure time for suitable electrical characteristics of SnO_2 films. When the UV/O_3-exposure time was 30 minutes, the SnO_2 TFTs exhibited the highest electrical performance compared to TFTs without UV/O_3-exposure, with field-effect mobility of 10.1 $cm^2\ V^{-1}\ s^{-1}$ and on/off ratio of 1.2×10^6 resulting from the enhanced M-O-M network, mass density, and oxygen vacancies of films. In contrast, the SnO_2 TFTs treated with UV/O_3 exposure time for 60 minutes show inferior field-effect mobility of 6.15 $cm^2\ V^{-1}\ s^{-1}$ and on/off ratio of 2.2×10^4, which is lower than TFTs without UV/O_3-exposure, because M-O-M network and mass density decreased and oxygen vacancies were excessively increased. Furthermore, significant changes were not observed in the SnO_2 (Sn^{4+}) phase, thickness, or surface morphology of SnO_2 films irrespective of UV/O_3-exposure time. The SnO_2 TFT exposed to UV/O_3 for 30 minutes during the pre-annealing stage demonstrates superior electrical performance, adequate for use in high-resolution active-matrix LCDs or OLED displays that demand a high field-effect mobility (>10 $cm^2\ V^{-1}\ s^{-1}$) and on/off ratio (>10^6).

Acknowledgments

This research was supported by the Basic Science Research Program through the National Research Foundation of Korea (NRF) funded by the Ministry of Science and ICT (2018R1A2B6008815). This research was also supported by the KIAT (Korea Institute for Advancement of Technology) grant funded by the Korea Government (MOTIE: Ministry of Trade Industry and Energy) (No. P0001018, HRD program for cutting-edge sensor).

ORCID iDs

Jaewon Jang https://orcid.org/0000-0003-1908-0015
Jin-Hyuk Bae https://orcid.org/0000-0003-3217-1309

References

[1] Kamiya T and Hosono H 2010 Material characteristics and applications of transparent amorphous oxide semiconductors *NPG Asia Mater.* **2** 15–22
[2] Wager J F 2003 Transparent electronics *Science* **300** 1245–7
[3] Nomura K, Ohta H, Ueda K, Kamiya T, Hirano M and Hosono H 2003 Thin-film transistor fabricated in single-crystalline transparent *Science* **300** 1269–73
[4] Hosono H 2006 Ionic amorphous oxide semiconductors : material design, carrier transport, and device application *J. Non. Cryst. Solids* **352** 851–8
[5] Minami T 2005 Transparent conducting oxide *Semicond. Sci. Technol.* **20** S35–44
[6] Minami T 2000 New n-type transparent conducting oxides *MRS Bull.* **25** 38–44
[7] Kwon J Y, Lee D J and Kim K B 2011 Review paper: transparent amorphous oxide semiconductor thin film transistor *Electron. Mater. Lett.* **7** 1–11
[8] Haxel G B, Hedrick J B and Orris G J 2002 *Rare Earth Elements—Critical Resources for High Technology* (National Minerals Information Center, Reston, Virginia: U.S. Geological Survey)
[9] Kim S J, Yoon S and Kim H J 2014 Review of solution-processed oxide thin-film transistors *Jpn. J. Appl. Phys.* **53** 02BA02
[10] Jang J, Kitsomboonloha R, Swisher S L, Park E S, Kang H and Subramanian V 2013 Transparent high-performance thin film transistors from solution-processed SnO_2/ZrO_2 gel-like precursors *Adv. Mater.* **25** 1042–7
[11] Jang B, Kim T, Lee S, Lee W, Kang H, Cho C S and Jang J 2018 High performance ultrathin SnO_2 thin-film transistors by Sol–Gel method *IEEE Electron Device Lett.* **39** 1179–82
[12] Priyadarshini D M, Mannam R, Rao M S R and Dasgupta N 2017 Effect of annealing ambient on SnO_2 thin film transistors *Appl. Surf. Sci.* **418** 414–17
[13] Sheng J, Choi D, Lee S, Park J and Park J 2016 Performance modulation of transparent ALD indium oxide films on flexible substrates : transition between metal-like conductor and high performance semiconductor states *J. Mater. Chem.* C **4** 7571–6
[14] Chiang H Q, Wager J F, Hoffman R L, Jeong J and Keszler D A 2005 High mobility transparent thin-film transistors with amorphous zinc tin oxide channel layer *Appl. Phys. Lett.* **86** 013503
[15] Kwack Y and Choi W 2013 Electrohydrodynamic jet spraying technique for oxide thin-film transistor *IEEE Electron Device Lett.* **34** 78–80
[16] Kim Y, Heo J, Kim T, Park S, Yoon M, Kim J, Oh M S, Yi G, Noh Y and Park S K 2012 Flexible metal-oxide devices made by room-temperature photochemical activation of sol–gel films *Nature* **489** 128
[17] Kwon J H, Choi J H, Bae J H and Park J 2019 Hysteresis reduction for organic thin film transistors with multiple stacked functional zirconia polymeric films *Crystals* **9** 634
[18] Avis C, Hwang H R and Jang J 2014 Effect of channel layer thickness on the performance of indium-zinc-tin oxide thin film transistors manufactured by inkjet printing *ACS Appl. Mater. Interfaces* **6** 10941–5

[19] Park J I, Jeong H S, Kim D K, Jang J, Kang I M, Lang P, Kim Y H, Kim H and Bae J H 2019 Importance of blade-coating temperature for diketopyrrolopyrrole-based thin-film transistors *Crystals* **9** 346
[20] Kim D K, Jeong H S, Kim Y R, Kwon H B, Kang S W and Bae J H 2018 Enhanced electrical properties in solution-processed InGaZnO thin-film transistors by viable hydroxyl group transfer process *Jpn. J. Appl. Phys.* **57** 05GC02
[21] Kim S J, Yoon S and Kim H J 2014 Review of solution-processed oxide thin-film transistors *Jpn. J. Appl. Phys.* **53** 02BA02
[22] Kim G H, Shin H S, Ahn B D, Kim K H, Park W J and Kim H J 2009 Formation mechanism of solution-processed nanocrystalline InGaZnO thin film as active channel layer in thin-film transistor *J. Electrochem. Soc.* **156** H7–9
[23] Kwon J M, Jung J, Rim Y S, Kim D L and Kim H J 2014 Improvement in negative bias stress stability of solution-processed amorphous In−Ga−Zn−O thin-film transistors using hydrogen peroxide *ACS Appl. Mater. Interfaces* **6** 3371–7
[24] Park W, Son I, Park H, Chung K, Xu Y, Lee T and Noh Y 2015 Facile routes to improve performance of solution-processed amorphous metal oxide thin film transistors by water vapor annealing *ACS Appl. Mater. Interfaces***7** 13289–94
[25] Ji K H, Kim J I, Jung H Y, Park S Y, Choi R, Kim U K, Hwang C S, Lee D, Hwang H and Jeong J K 2011 Effect of high-pressure oxygen annealing on negative bias illumination stress-induced instability of InGaZnO thin film transistors *Appl. Phys. Lett.* **98** 103509
[26] Rim Y S, Jeong W H, Kim D L, Lim H S, Kim K M and Kim H J 2012 Simultaneous modification of pyrolysis and densification for low-temperature solution-processed flexible oxide thin-film tranasistors *J. Mater. Chem.* **22** 12491
[27] Mativenga M, Choi J W, Hur J H, Kim H J and Jang J 2011 Highly stable amorphous indium–gallium–zinc-oxide thin-film transistor using an etch-stopper and a via-hole structure *J. Inf. Disp.* **12** 47–50
[28] Lee W Y, Ha S H, Lee H, Bae J H, Jang B, Kwon H J and Jang J 2019 Densification control as a method of improving the ambient stability of Sol–Gel-processed *IEEE Electron Device Lett.* **40** 905–8
[29] Kim J-H, Ma J, Lee S, Jo S and Kim C S 2019 Effect of ultraviolet–ozone treatment on the properties and antibacterial activity of zinc oxide Sol-Gel film *Materials* **12** 2422
[30] Vig J R 1985 UV/ozone cleaning of surfaces *J. Vac. Sci. Technol.* A **3** 1027
[31] Jadhav H, Suryawanshi S, More M A and Sinha S 2017 Pulsed laser deposition of tin oxide thin films for field emission studies *Appl. Surf. Sci.* **419** 764–9
[32] Liang L Y, Liu Z M, Cao H T and Pan X Q 2010 Microstructural, optical, and electrical properties of SnO thin films prepared on quartz via a two-step method *ACS Appl. Mater. Interfaces* **4** 1060–5
[33] Hwang Y H, Seo J, Yun J M, Park H, Yang S, Park S K and Bae B 2013 An 'aqueous route' for the fabrication of low-temperature-processable oxide flexible transparent thin-film transistors on plastic substrates *NPG Asia Mater.* **5** e45
[34] Birkholz M 2006 *Thin Film Analysis by X-Ray Scattering* (Weinheim: Wiley-VCH)
[35] Veldhuis S A, Brinks P, Stawski T M, Göbel O F and Ten Elshof J E 2014 A facile method for the density determination of ceramic thin films using X-ray reflectivity *J. Sol-Gel Sci. Technol.* **71** 118–28
[36] Noh H-K, Chang K J, Ryu B and Lee W J 2011 Electronic structure of oxygen-vacancy defects in amorphous In-Ga-Zn-O semiconductors *Phys. Rev.* B **84** 115205
[37] Kamiya T, Nomura K, Hirano M and Hosono H 2008 Electronic structure of oxygen deficient amorphous oxide semiconductor a-$InGaZnO_{4-x}$: optical analyses and first-principle calculations *Phys. Status Solidi* c **5** 3098–100
[38] Zhai J, Zhang X, Hai F S, Yu X, Zhu R and Zhang W 2014 Fabrication and characterization of thin-film transistors with SnO_2 channel by spray pyrolysis *Jpn. J. Appl. Phys.* **53** 10–13
[39] Zhang X A, Zhai J X, Yu X K, Zhu R J and Zhang W F 2015 Effect of annealing temperature on the performance of SnO_2 thin film transistors prepared by spray pyrolysis *J. Nanosci. Nanotechnol.* **15** 6183–7
[40] Lee H, Ha S, Bae J H, Kang I M, Kim K, Lee W Y and Jang J 2019 Effect of annealing ambient on SnO_2 thin film transistors fabricated via an ethanol-based Sol-Gel route *Electron* **8** 1–9
[41] Huang G, Duan L, Dong G, Zhang D and Qiu Y 2014 High-mobility solution-processed tin oxide thin-film transistors with high-κ alumina dielectric working in enhancement mode *ACS Appl. Mater. Interfaces* **6** 20786–94